[16] Ph. M. Morse:“Vibration and Sound“,McGraw-Hill Book Company, INC., 1948

[17] N. Kroll, R. Radespiel, C.-C. Rossow:“Accurate and Efficient Flow Solver for 3D Applications on Structured Meshes“ Lecture Series 1994. Computational Fluid Dynamics, Von Karman Institute of Fluid Dynamics, 1994

[18] K. J. Schultz, D. Lohmann, J. A. Lieser, K. Pahlke:“Aeroacoustic Calculations of Helicopter Rotors at DLR“, Paper No. 29, AGARD Symposium on Aerodynamics and Aeroacoustics of Rotorcraft, Berlin, October 10 - 14, 1994

[19] M. Kuntz, D. Lohmann, J. A. Lieser, K. Pahlke:“Comparison of Rotor Noise Predictions obtained by a Lifting Surface Method and Euler Solutions using Kirchhoff Equation“, CEAS/AIAA, Paper No. 95-136, 1995

[20] TASCflow3D:“Technical Summary of ASC‘s CFD Technology“ Advanced Scientific Computing Ltd., Waterloo, Ontario, Canada, 1992

[21] B. E. Launder, D. B. Spalding:“The Numerical Computation of Turbulent Flows“, Comput. Methods Appl. Mech. and Eng., Vol. 3, pp. 269 - 289, 1974

[22] H. Capdevila, J. Pharoah:“ Computational Fluid Dynamics Analysis of Axial Flow Fans for Automotive Cooling Systems“, Presented at CFD ,95, Third Annual Conference of the CFD Society of Canada, Banff, Alberta, Canada, June 25 - 27, 1995

[23] J.-C. Rotta:“FORTRAN Rechenprogramm für Grenzschichten bei kompressiblen und achsensymme trischen Strömungen“, DLR-FB 71-51, 1971

[24] H. Schlichting:“Boundary Layer Theory“, Verlag G. Braun, Karlsruhe, Card No. 67-29199, 1968

[25] P. Lavrich, J. Simonich, D. Mc Cormick:“An Assessment of Wake Structure Behind Forward Swept and Aft Swept Propfans at High Loading“, DGLR/AIAA 14th Conference, Aachen, Germany, May 11 - 14, 1992

[26] D. Lohmann:“Aeroakustische Optimierung eines Kfz-Gebläses“, represented at the meeting: ‚Akustik und Aerodynamik des Kraftfahrzeugs‘, Haus der Technik e. V., Essen, Germany, 1 - 2 February, 1994, edited by the Expert Verlag GmbH, Renningen, ISBN 3-8169-1190-0, 1995

[27] U. Stark:“Strömungsuntersuchungen an gepfeilten Verdichtergittern bei kompressibler Unterschallströmung“, DLR-FB 67-09 January 1967

[28] U. Stark:“Untersuchungen über den Einfluß der Machzahl und der Pfeilung auf die Sekundärverluste in Verdichtergittern bei hohen Unterschallgeschwindigkeiten“, DLR-FB 69-55, June 1969

[29] W. R. Godwin:“Effect of Sweep on Performance of compressor Blade Sections as Indicated by Swept-Blade Rotor, Unswept-Blade Rotor, and Cascade Tests“, TN 4062, Washington, July 1957

[30] L. H. Smith, H. Yeh:“ Sweep and Dihedral Effects in Axial-Flow Turbomachinery“, Journal of Basic Engineering, Transactions of the ASME, pp. 401 - 416, September 1963

[31] M. G. Beiler:“Untersuchungen der dreidimensionalen Strömung durch Axialventilatoren mit gekrümmten Schaufeln“, VDI Verlag, Reihe 7, Strömungstechnik Nr. 298, ISBN 3-18-329807-4, 1996

[32] M. V. Lowson:“Airfoil Noise Radiation Models“ CEAS/AIAA Paper No. 95-123, 1995

[33] S. Akishita, K. Ohtsuta:“Broad Band Noise from an Isolated Two Dimensional Airfoil:, 10th AIAA Con ference, Seattle, Washington, July 9 - 11, 1986

[34] M. V. Lowson:“Noise due to Boundary Layer Instabilities“, CEAS/AIAA Paper No. 95-124, 1995

[35] H. W. Stock, W. Haase:“Determination of Lengts Scales in Algebraic Turbulence Models For Navier-Stokes Methods“, AIAA Journal, Vol. 27, No. 1, pp. 5-14, January 1989

field noise. Input data are the aerodynamic pressure and boundary layer thickness distribution which were computed with the LBS code too. The prediction accuracy for the periodic noise is within 3 dB. The random noise was computed with the LBS code too. The finally computed and dB(A)-weighted overall noise levels agree with the experiment by a difference of about 1 dB(A).

ACKNOWLEDGEMENT

The authors wish to acknowledge Mr. H. Bleecke for the computation of the FLOWer code grid logic and J. Fassbender for software engineering support in computing the boundary layer thickness. The authors are indebted to Dipl.-Ing. W. Bookjans for performing the radial-equilibrium calculations.The authors also achnowledges the technical staff of Siemens Elctric Ltd. for the excellent conduction of the aeroacoustic experiments.

REFERENCE

[1] S. Sarin, S. Canard-Caruana, P. Cloarec, R. Donelly, D. Lohmann, S. Mejer, J. Schulten:“Comparitive In vestigation of Predictive Capability of Aeroacoustic Methods of Single Rotation Propellers“, GARTEUR (Group of Aeronautical Research and Technology in Europe), Techn. Rep. TP077, 1993

[2] D. Lohmann:“Prediction of Ducted Radiator Fan Aeroacoustics With a Lifting Surface Method“, DGLR/AIAA 14th Aeroacoustic Conference, Proc. pp 576 - 606, Aachen, Germany, May 11-14, 1992

[3] D. Lohmann:“Numerical Optimization of Propeller Aeroacoustics - Using Evolution Strategy“, International Noise and Vibration Control Conference Noise-93, Proceedings Volume 1, pp. 103 - 114, St. Petersburg, Russia, May 31 - June 3, 1993

[4] W. Eversman: „Radiated Noise of Ducted Fans“, DGLR/AIAA 14th Aeroacoustics Conference, Proc. pp. 836 - 845, Aachen, Germany, May 11 - 14, 1992

[5] W. Eversman, I. D. Roy: "Ducted Fan Aeroacoustic Radiation Including the Effects of Nonuniform Mean Flow and Acoustic Treatment", AIAA Paper No. 93-4424, October , 1993

[6] Y. Ozyoruk, L. N. Long: „A Navier-Stokes/Kirchhoff Method for Noise Radiation from Ducted Fans“, 32nd Aerospace /Sciences Meeting & Exhibit, AIAA Paper No. 94-0462, Reno, USA, January 10 - 13, 1994

[7] Y. Ozyoruk, L. N. Long:“ Computation of Sound Radiation from Engine Inlets“, First CEAS/AIAA Aeroacoustics Conference, CEAS/AIAA Paper No. 95-063, Pennsylvania, USA, June 12 - 15, 1995

[8] C. H. Hsu, P. L. Spence:“Ducted Fan Noise Prediction Based on a HybridAerodynamic-Aeroacoustic Technique“, First CEAS/AIAA Aeroacoustics Conference, CEAS/AIAA Paper No. 95-075, Pennsylvania, USA, June 12 - 15, 1995

[9] Y. Ozyoruk, L. N. Long:“Progress in Time-Domain Calculaltions of Ducted Fan Noise: Multigrid Acceleration of a High-Resolution CAA Scheme“, 2nd AIAA/CEAS Aeroacoustics Conference, CEAS/AIAA Paper No. 96-1771, PA, USA, May 6 - 8, 1996

[10] J. M. Tyler, T. G. Sofrin:“Axial Flow Compressor Noise Studies“, S.A.E.-Meeting Paper No. 345-D, 1961

[11] M. K. Myers:“Boundary Integral Formulations for Ducted Fan Radiation Calculations“, First Joint CEAS/AIAA Aeroacoustics Conference, CEAS/AIAA Paper No. 95-076, Pennsylvania, USA, June 12 - 15, 1995

[12] R. Martinez:“Aeroacoustic Diffraction and Dissipation by a Short Propeller Cowl in Subsonic Flight“, Cambridge Acoustical Associated Report U-2065-385, June, 1995

[13] Th. Carolus,Th. Fuest, M. Beiler:“Broad Band Noise Prediction of Low Pressure Axial Flow Fans Employing CFD-Flow Field Data“, CEAS/AIAA, Paper No. 95-022, 1995

[14] S. A. L. Glegg:“Broadband Noise from Ducted Prop Fans“, 15th AIAA Confernce, Long Beach, CA, Paper No. 93-4402, October 25 - 27, 1993

[15] K. S. Brentner:“Prediction of Helicopter Rotor Discrete Frequency Noise“, NASA Technical Memorandum 87721, October 1986

being dominated by the random noise parts and covering the periodic noise. Both tendencies are well predicted in the computed polar diagrams of Fig. 17 The color of the calculated periodic noise contour plots is slightly different from the experimental plots because these noise levels are overpredicted.

CONCLUDING REMARKS

Four different approaches to compute the performance of a forward swept lowspeed radiator fan are compared for validation:

1. 3-D Navier Stokes computation with the DLR code FLOWer

2. 3-D Navier Stokes computation with the Siemens Electric code TASCflow

3. Lifting surface panel calclulation with the DLR 3-D code LBS

4. Radial equilibrium calculation with the 3-D cascade flow method RE

The first 2 methods are non-linear methods, whereas the second 2 methods are linear methods. Comparing the results of the different methods against each other and with the experimental data it is noted that the first two non-linear methods provide the superior results. The static pressure and the efficiency are quite well predicted within a flow coefficient range, where the efficiency decays from the maximum towards the right-hand side branch.

The discrepancies between experiment/theory at free stream condition are probalbly firstly caused by the simplified grid topology using coaxial cylinders for the hub and duct and secondly by the definition of an undisturbed onset flow. Here the real flow is assumed to be already separated at the fan face instead of being undisturbed. The discrepancies could be avoided by the definition of a more realistic geometry and an unsteady onset flow. The linearized panel method LBS, modeling the real fan geometry, is the only method, which calculates a satisfying static pressure coefficient at free stream condition. Also the radial equilibrium RE method, recently used for the aerodynamic design, delivers satisfying data for the the performance at the free stream condition.

Further investigations were made with the FLOWer code to test the prediction capability of special flow effects which appear in the case of forwart and aft swept fans. For this test a second, aft swept fan was computed and analysed. The results, which are compared with the results from the forward swept fan agree well with the experience from earlier experiments.

To validate the linear methods with the CFD code FLOWer local values as pressure, lift, drag and boundary layer thickness distributions have been succesfully compared. The agreement is qualitatively good and is encouraging to use furtherly the linear methods for fan design.

It was attempted to perform different acoustic computations for periodic and stochastic fan noise. The application of the DLR Kirchhoff method failed because the Navier Stokes code FLOWer cannot resolve the acoustic near-field at the fan face at low Mach numbers. Therefore, for future lowspeed computations with the Kirchhoff method a higher-order scheme has to be applied. The aeroacoustic comptation with the LBS code using the acoustic analogy for the near-field and Rayleigh‘s formular for the far-field delivered good results for the periodic far-

quency BPF and the overall sound pressure level including both, the periodic and broadband noise is shown in Fig. 15.

The agreement of the noise levels is quite satisfactory. It should be noted that the accuracy of the prediction is within 3 dB for the BPF and within 1 dB(A) for the overall noise level.

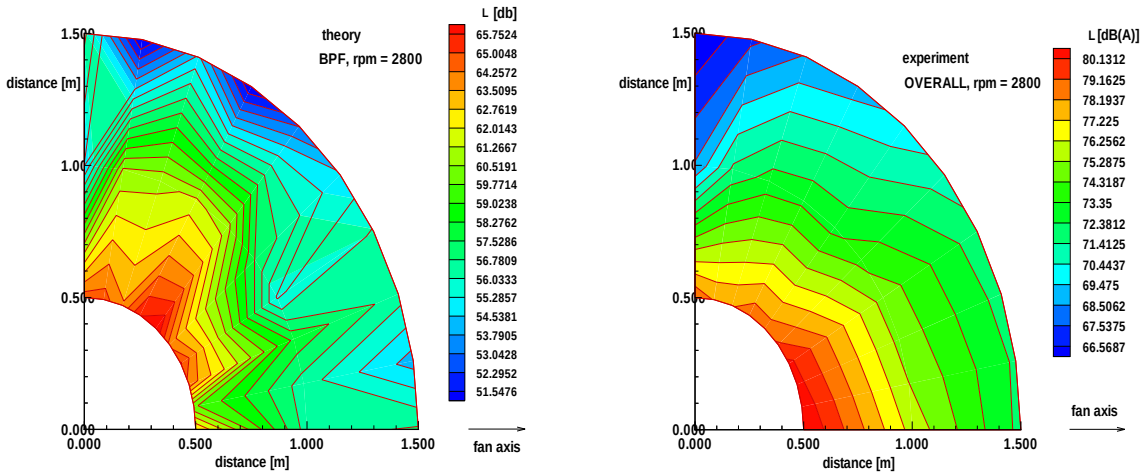

(a) (b)

Fig. 16 Measured sound field around the fan, (a) BPF sound pressure level, (b) overall sound pressure level

A second comparison at free stream condition but different microphone locations was conducted at 2800 rpm which is represented in Fig. 16 and Fig. 17. The pictures are contour plots that indicate the maximum noise level radiation direction. The periodic fan noise radiates

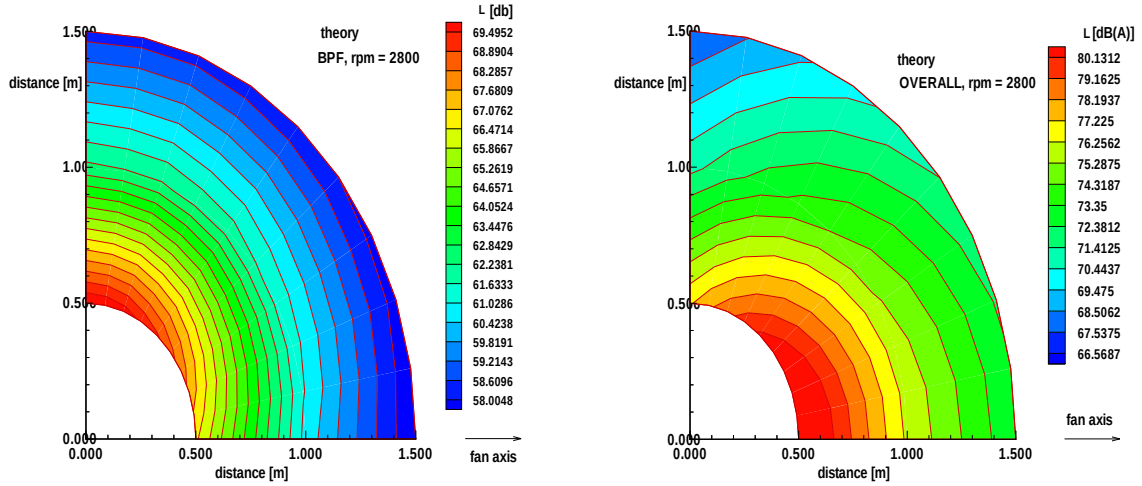

(a) (b)

Fig. 17 Computed sound field around the fan, (a) BPF sound pressure level, (b) overall sound pressure level

mainly towards the rotor plane. The overall noise level has its maximum in the axial direction,

were measured on axis and in a distance of d = 1 m from the fan face are represented in Fig. 13. The spectra show that the periodic noise is to be realized up to the second harmonic. Higher harmonics are hided by the broad band spectrum. In most cases the first harmonic (not the BPF !) has the highest sound pressure level. This also is a typical sign which indicates that the sound source has a monopole or quadrupole character.

The broad band spectrum is characterized by white noise. From the CFD analysis follows that the white noise part is probably caused by separated flow..

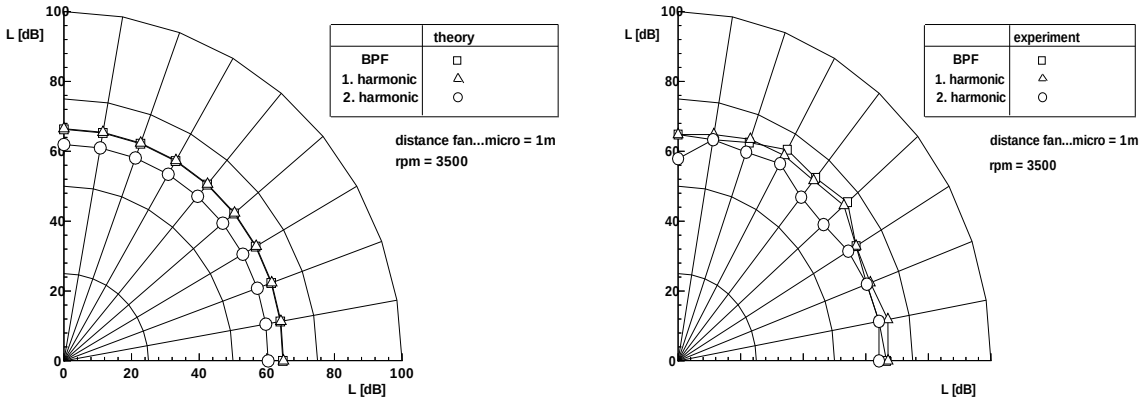

(a) (b)

Fig. 14 Polar diagram of the BPF and the first 2 harmonics, (a) theory, (b) experiment

The acoustic computations were performed with the LBS code on CRAY XMP computer. The CPU time needed for the periodic noise calculations is about 1 hour. The calculations of the stochastic noise part took 5 CPU minutes only. Fig. 14 compares the computed sound pressure levels of the BPF, 1st and 2nd harmonic with the measured sound pressure levels at free stream condition and at 1 m distance from the fan face.

A further comparison experiment/theory of the sound pressure level of the blade passage fre-

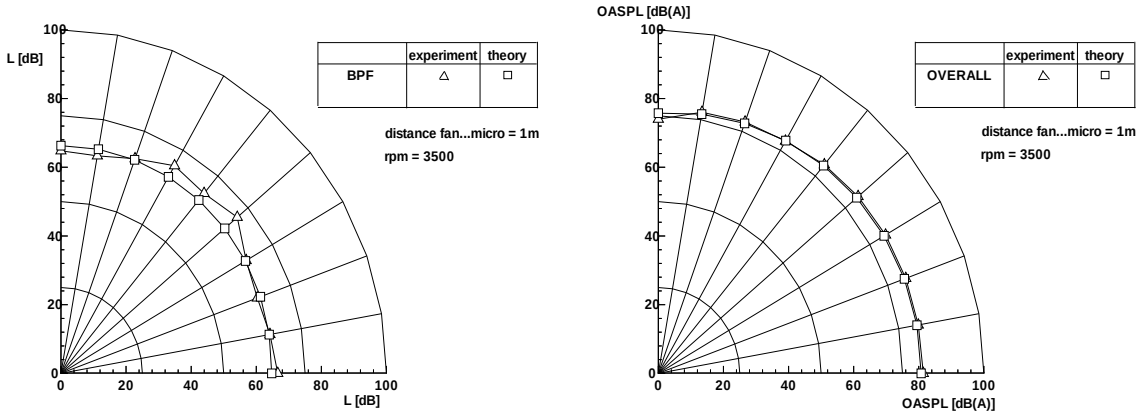

(a) (b)

Fig. 15 Comparison experiment/theory, (a) BPF sound pressure level, (b) overall sound pressure level

Acoustic signatures of low speed fans are often characterized by the typical curvature of a monopole or quadrupole time history. An example of a 3-bladed fan with rectangular blade

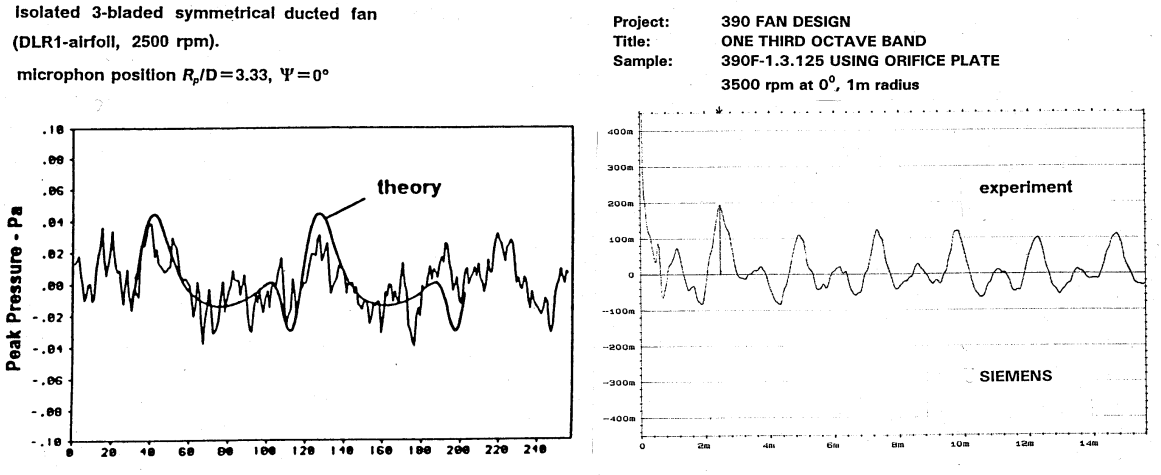

(a) (b)

Fig. 12 Similarity of acoustic signatures, (a) signature of a 3-bladed fan with rectangular planform (esperiment/theory [2]), (b) signature of a 7-bladed forward swept fan of Siemens Electric Ltd. (experiment)

planform is demonstrated in Fig. 12(a).The periodic noise part of the measured signature is overlapped by stochastic signals. A second curve is shown which represents the pure periodic part of the signature resulting from a time averaging procedure. This second curve demonstrats the typical feature of a monopole or quadrupole type source. A similar signature was measured at the 7-bladed forward swept fan of this study (see Fig. 12(b)).

The acoustic experiments were conducte with 2800 and 3500 rpm for the 7-bladed forward swept fan at free stream condition. A narrow band and a third octave band spectrum which

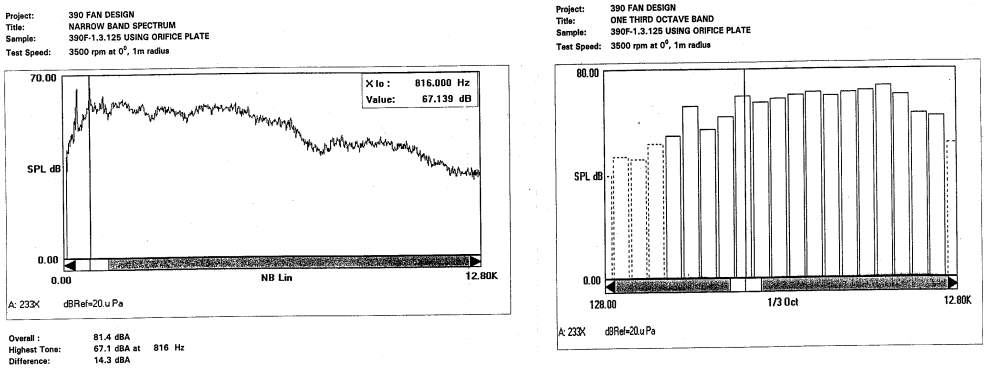

(a) (b)

Fig. 13 Measurd sound spectra at free stream condition (rpm = 3500, d = 1 m) , (a) narrow band spectrum, (b) thierd octave band spectr

θ is the arc coordinate in circumferential direction within the plane of the fan face, ω is the circular frequency and ρ is the density. The pressure in the far-field is:

$$dp_f = -\frac{i\omega\rho v_z e^{-ikh}}{2\pi h} dS \tag{5}$$

where k is the wave number, h is the distance between the source and the observer and dS is a surface element at the fan face. The acoustic far-field pressure is obtained by integration on the surface at the fan face:

$$p_f = \frac{1}{2\pi}\int_{r_b}^{r_a}\int_0^{2\pi}\sum_{n=0}^{\infty}\frac{\Delta p_z}{\Delta z}\frac{e^{-i(kh+m\theta)}}{h} r\,d\theta\,dr \tag{6}$$

(Rayleigh's formula). For the far-field computation the distance h can be approximated by $h \cong d - \cos\theta\sin\psi$ so that from equation (5) follows

$$p_f = \frac{e^{-ikd}}{h}\int_{r_b}^{r_a}\sum_{n=0}^{\infty} i^m \frac{\Delta p_n}{\Delta z} J_m(kr\sin\psi)\,r\,dr \tag{7}$$

J_m is the Bessel function of the order of m =nB, where B is the blade number. The far-field pressure p_f is calculated numerically using Simpson's rule.

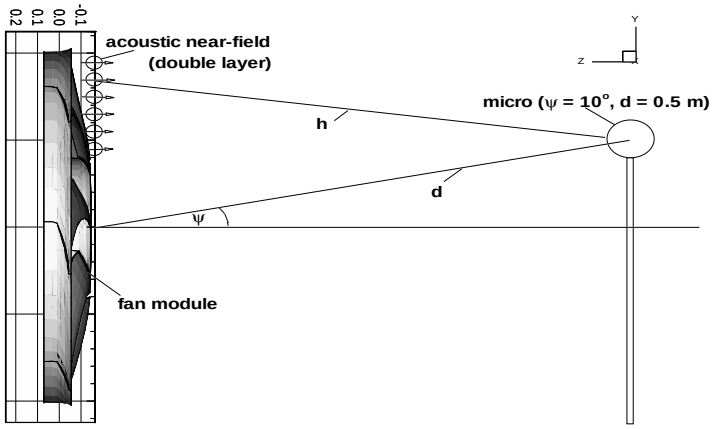

Fig. 11 Computational model for lowspeed fan acoustics using acoustic analogy

Originally the goal of this study was to apply the Kirchhoff method too. Here the idea was to compute the acoustic far-field from a Kirchhoff surface which is located at the fan face. The near-field sources on the Kirchhoff surface are the result of the Navier Stokes computation. Because the Navier Stokes code computes separated flow, we even supposed to obtain stochastic noise parts too. However, the computational terms of the FLOWer code are of third order only which is accurate enough for aerodynamics but not for acoustics. Thus we got the same answer from the DLR code APSIM applying the Kirchhoff method as from the direct computation of the far-field with the LBS code: All the acoustic signals cancel each other in the far-field. Again the phase differences are very small.

ration on the whole pressure side of the airfoil. On the suction side the flow is attached. The comparison of the 3 different calculated boundary layer thickness-distributions over the airfoil can be seen in Fig. 8(b).

Acoustics

Basically, each body immersed in a flow generates sound whose intensity increases with the speed of the flow. Essential causes of the generated noise are the volume displacement, called thickness or monopole effect, the drag and lift forces or dipole effect, fluctuating pressures due to flow instabilities and vorticity on the blade or in the wake and flow separation which can be partly modeled by dipoles and quadrupoles. All the periodic noise parts can be calculated with the acoustic analogy when the source strength is known. Here, the source strength is obtained from an earlier performed aerodynamic computation. On the other side, the computation of the stochastic noise parts can only be performed by the use of half-empirical models which use acoustic results from 2-D airfoils. Both noise computation have to be performed separately [2].

The use of the acoustic analogy becomes difficult when the Mach number is low. The main problem rises from the computation of the acoustic far-field. Interference effects caused by the different blades of a multi-bladed fan will cancel the acoustic signals so that only a few decibels remain from the original sound pressure level. In general the problem appears, when the retarded time differences which are caused by different distances between the source and the observer vanish in the acoustic far-field. Then the acoustic signatures degenerate to simple sine waves with the consequence that in the case of many equally spaced rotor blades the acoustic signals cancel each other. However, the local differences between the source and the observer are significantly larger in the near-field. Therefore, at low Mach numbers it is necessary, to firstly compute the acoustic near-field at the fan face. For this reason a double layer of sources has to be calculated which can be computed with the acoustic analogy method as e.g. Farassat type 1 including a quadrupol term for boundary layer effects.

The second part to compute the far-field is comparable with the computation of duct acoustics of Tyler and Sofrin [10] or Morse‘s formular for a piston in a wall [16]. Rayleigh‘s formular has to be used considering the fan face as a piston membran to compute the acoustic far-field. This is the key of the LBS method to compute the acoustics of a fan at low Mach numbers. The computational procedure is the following:

Firstly, the particle velocity of the sources can be obtained by a gradient normal to the fan face surface

$$v_z = -\frac{1}{i\omega\rho}\mathrm{grad}_z p_{LBS} \tag{3}$$

(see Fig. 11). Here p_{LBS} is the calculated acoustic near-field pressure which can be developed into a Fourier series so that

$$v_z = -\frac{1}{i\omega\rho}\sum_{n=0}^{\infty}\frac{dp_n}{dz}e^{im\theta} \tag{4}$$

Navier Stokes Code offers a first possibility to validate the LBS code with local values. It should be mentioned that these locations are essential for the acoustics because the blade is nearby the hub and duct where unsteady aerodynamic interactions between the blade and the surrounding appear which can cause intensive sound sources. The coarse panel grid is used here to save computer time, e.g. during the optimization (This is the same grid which is used for the acoustic calculations). The peak pressures values at the leading edge have strong gradi ents which lead to important sound sources and should normally be avoided [2]. The wiggles at the trailing edge are probably caused by the thick end of the airfoil. Fortunately the peak values are decreasing in spanwise direction towards outboard which means a decreasing noise source towards the tip.

A second comparison is presented in Fig. 9 which shows the load respectively the lift and drag distribution over the radius. At free stream condition the lift is very low. The agreementbetween both calculations is acceptable, the curves agree well in the slope and size, here especially at the tip. The integral values differ slightly. Also the wall effects are taken into account so that the lift is neither zero at the hub nor at the tip. The RE method result shows basically the same tendency as in the upper figures but overpredicts those values.

Boundary layer thickness distributions

To compare the computed boundery layer, we selected a representative cut at the relative radius station r/R = .8. As test case again the free stream condition is chosen. The boundary layer thickness is computed from the laminar computational result of the CFD code FLOWer according to the method presented in [35], from the result of the lifting surface code LBS and finally by the use of the well-known approximation for a flat plate:

$$\frac{\delta}{c} = \frac{5}{\sqrt{Re}} \tag{2}$$

Fig 10 represents a vector velocity diagram of the CFD result which shows a bubble and sepa

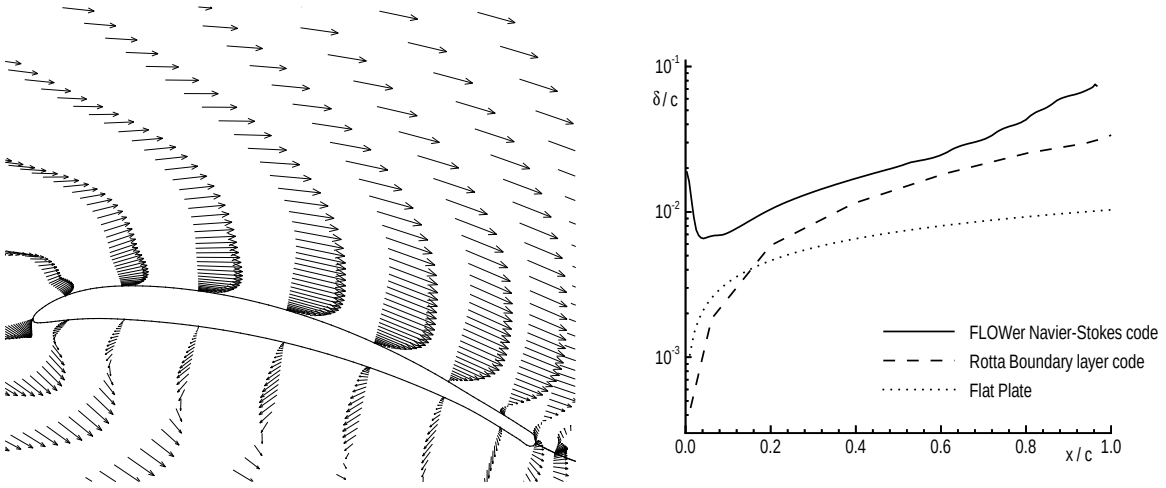

(a) (b)

Fig. 10 Calculated boundary layer thickness, (a) laminar computed velocity vector diagram at r/R = .8, (b) comparison of the different calculated boundary layer thickness

The main reason for the lack of locally measured data is the high price of pressure transducer installations and the additional electrical equipment which have not been investigated in the past. Here CFD flow field simulation can be a helpful tool to compute the wanted local aerody dynamic values as pressure, lift or drag distributions

Unfortunately only few experimental data exist for Reynolds numbers Re < 300.000 [32, 33]. This Re range is dominated by large scale laminar flow effects as bubbles or boundary layer in stabilities in the separated shear flow near the trailing edge [34]. Bubbles near the leading edge can cause transition from laminar to turbulent or separated flow. Also re-attachment can appear after laminar separation. However, experimental investigations with trip wires on the suction side of the fan blade to destroy a bubble have been without any success which indicates that the flow is more often stable than is supposed. Therefore, we assume the flow to be laminar up to the midchord and then slightly separated. This assumption is necessary because our NS code cannot compute mixed laminar/turbulent flow. A further simplification is the idealized geome try of constant duct/hub radii where the onset flow is axisymmetric and undisturbed. Pressure fluctuations or separated flow effects caused by great pressure gradients at the intake are not condidered in this computation.

Fig. 8 shows pressure distributions which were calculated with the DLR lifting surface code LBS and with the Navier Stokes code FLOWer at free stream condition. The pictures present a comparison which should approximatively prove, that the pressure distributions are well enough predicted for acoustic computations, especially nearby the hub and duct. Here the

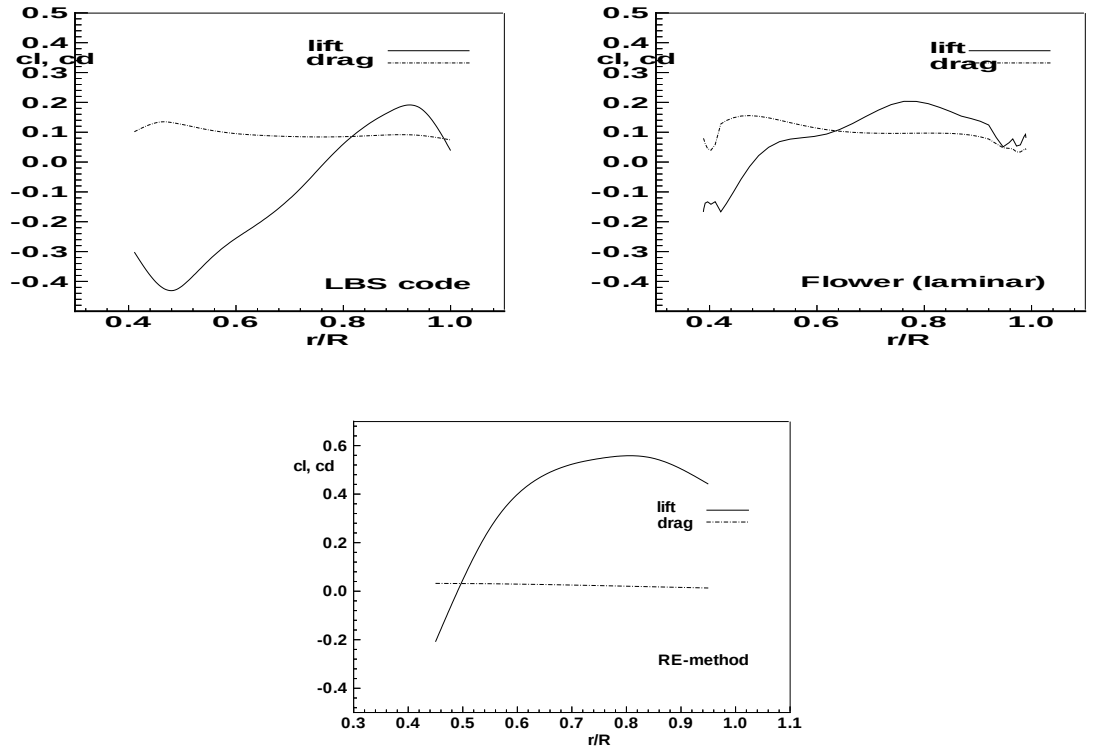

Fig. 9 Comparison of the calculated lift/drag distributions at free stream condition, left side: lifting surface code LBS (laminar, ψ = -.0017), right side : Navier Stokes code FLOWer (laminar, ψ =.0113), lower side: RE method (turbulent (ψ =.0267)

the swept blades generates a very complicated velocity field structure. The pictures which show airfoils are cuts at different radial stations. The radial stations are marked by arrows. The flow begins at the leading edge with a bubble (leading edge vortex) which gets smaller towards the tip and confirmes the statement of point 8. The flow on the pressure side is fully separated whereas the flow on the suction side is mainly attached. The streamlines after the trailing edge of the forward swept blade show a better distribution of the mass flow over the fan cross section. The streamlines of the aft swept fan indicate that the flow is displaced from the middle to the hub region which partly confirmes point 9. The boundary layer thicknes at the hub is inboth cases, forward and swept blades, about twice of the boundary layer of the airfoil.

Reserve flow at the hub cannot be observed. Because separation appears at all places of the fan blades the fan is supposed to be an effective white noise sound source.

Validation of the lifting surface code LBS for local aerodynamic data

In the following part of the study the acoustic measurements were conducted at free stream conditions, where the static pressure-ratio is approximately zero.

Pressure, lift and drag distributions

In general the aerodynamic data output of radiator fan experiments is given in form of integral values, which covers a lot of important informations. Especially for acoustics special local data are needed to detect sound sources caused by bubbles, vortices or separated flow phenomena.

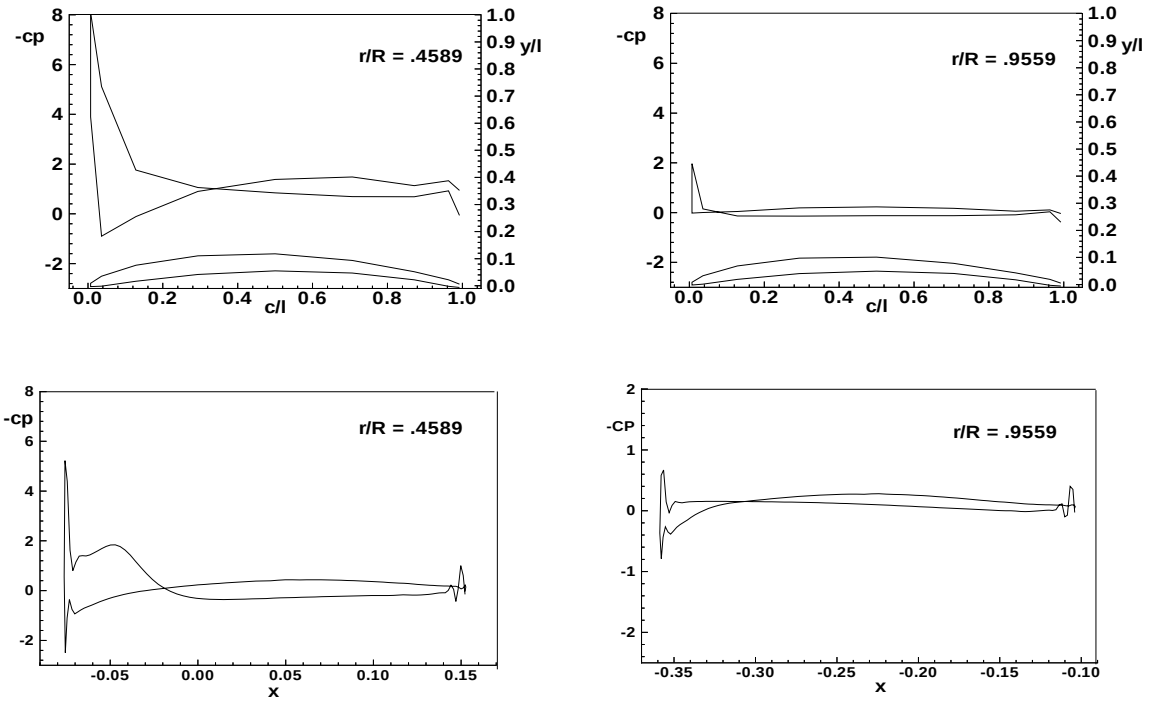

Fig. 8 Comparison of calculated pressure distributions at free stream condition, upper figures: lifting surface code LBS, lower figures: Navier Stokes code FLOWer (laminar)

In general swept blades have a more or less effective flow guidance and insofar a smaller effi ciency than e.g. rectangular blades. From point 1 through 10 follows that an opposite directed

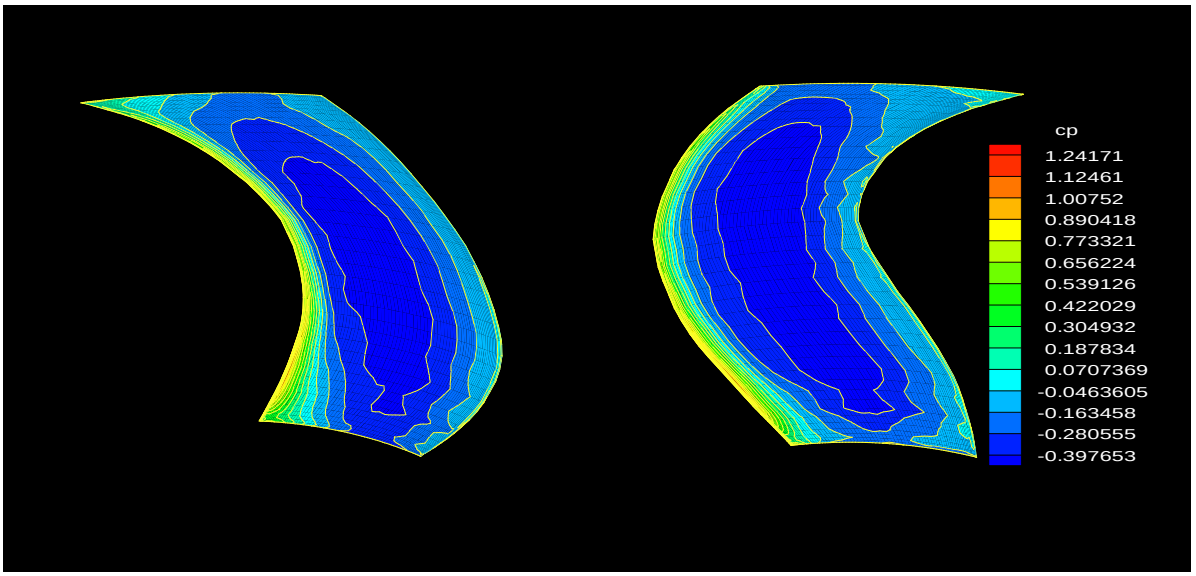

Fig. 6 With FLOWer code computed laminar pressure fields on the suction side of 2 different fans, left side: forward swept fan , right side: aft swept fan

sweep can cause an opposite flow behaviour. The pressure contour plots in Fig. 6 confirm the statements of point 1, 2 and 6, 7. The dark zones of the forward swept blade on the left side which are representative for the higher loads are shifted towards the trailing edge whereas the aft-swept blade on the right side shows the opposite behaviour. The load of the forward swept fan is also not so strong increasing towards the tip than the load of the aft swept fan. Therefore, because especially the tip region is a dominant noise generator the reduced load of the forward-swept fan can be an advantage in acoustics in comparison to the aft-swept fan.

Fig. 7 shows a Mach number contour plot of the forward and aft swept fan. The flow around

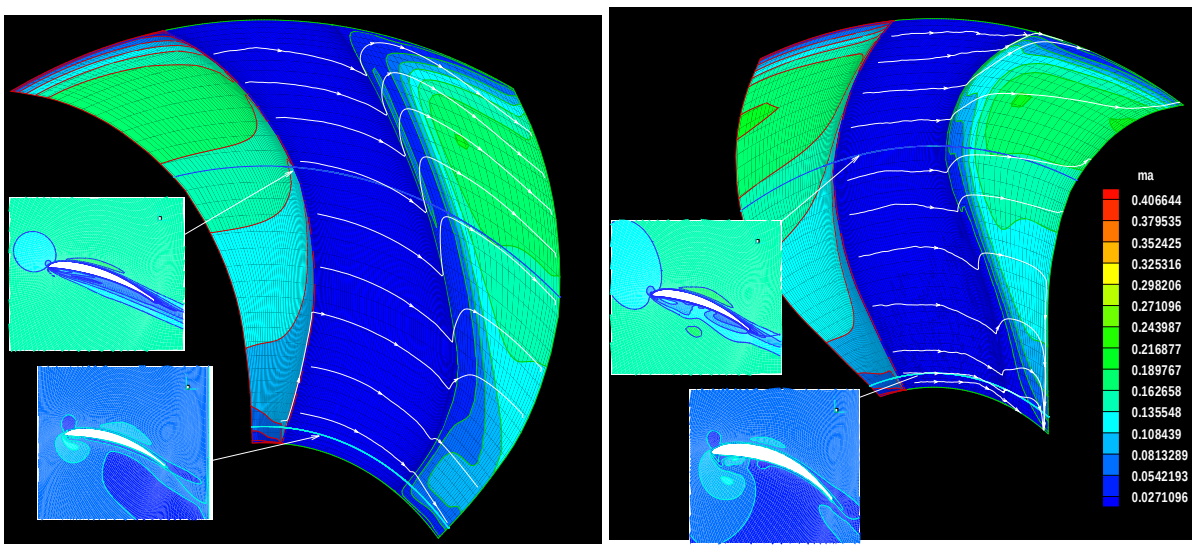

Fig. 7 With FLOWer code computed laminar Mach number contours of 2 different fans, left side: forward swept fan , right side: aft swept fan

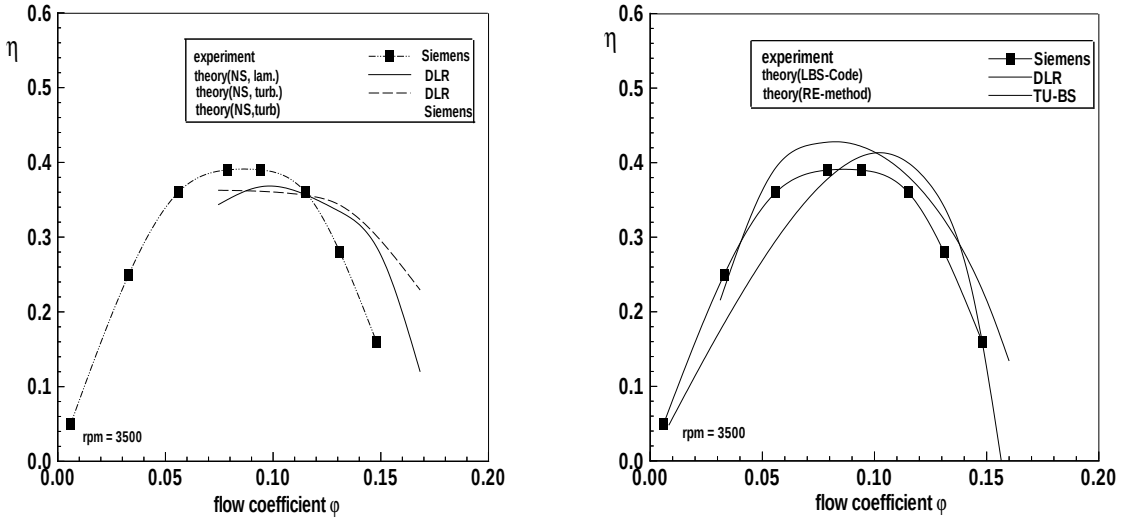

(a) (b)

Fig. 5 Comparison of the calculated static efficiency with experimental data, (a)Navier Stokes code FLOWer (inviscid, laminar and turbulent), (b) lifting surface code LBS and RE-method

More detailed information can be obtained by the flow field outwards the blade. For such a study we use the opportunity to consider a second fan with aft-swept blades. The fan should have the same geometric parameters up to the reverse sweep. Unfortunately, for an aft-swept fan we have no experimental data. Hence we can only compare computational results.

Firstly, we noted that the performances of both, forward and aft swept configurations differ only lttle by a small amount. However, in the paper of Lavrich et al [25] is shown, that the total pressure difference tends to go to zero if the load becomes smaller. Thus we assume that the differences must be small for the presented test case of a very low loaded fan. This is contrary to the local data of the flow field. Basically we know from our own investigations and from those of other authors [26, 27, 28, 29, 30, 31] the following special features of the flow field of a forward swept fan:

1) lower load at the L.E., higher load at the T.E
2) reduced load towards the tip
3) creased vorticity at the hub
4) higher flow rate in the tip region
5) reduced separation for higher loads

and of an aft swept fan

6) higher load at the L.E. and lower load at the T.E.
7) higher load at the tip, reduced Mach-number
8) L.E. vortex which reduces separation
9) higher flow rate in the hub region
10) increased separation for higher loads

ing a fully turbulent profile boundary layer, an additional trailing edge loss and a constant leak age flow of 15 %. No other losses were introduced and this may be the reason for the differences between the measured andpredicted results for medium and high φ-values. For low φ-values the differences are much higher. This may partly be attributed to the so-called F-profiles used, all being characterized by a small amount of nose camber (droop) in order to improve the high angle of attack performance. Obviously, this is a good idea but has not yet been incorporated into the theory.

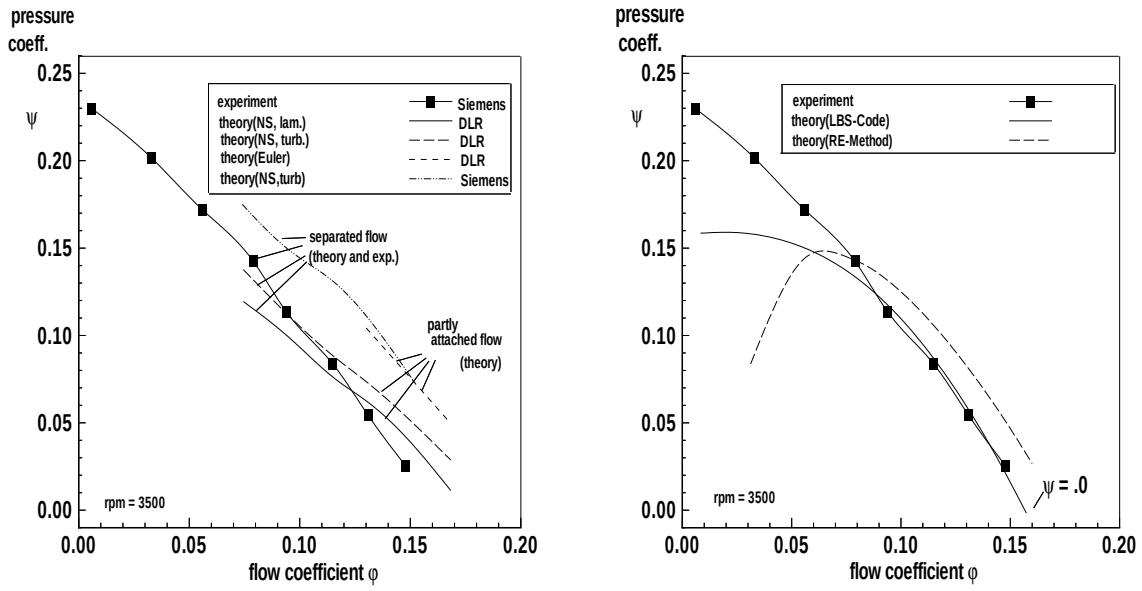

(a) (b)

Fig. 4 Comparison of static pressure difference with experimental data, (a) Navier Stokes code FLOWer (inviscid, laminar and turbulent), (b) lifting surface code LBS and RE-method

The static efficiency is presented in Fig. 5. The CFD computed results correspond satisfying in the maximum values. However, again the right branches of the theoretical curves are shiftet towards higher flow coefficients as can be seen at the static pressure. This appears when the theoretical and the experimental fan model differ in the trailing edge angles definition at the blade. Therefore, the difference can be compensated by considering larger pitch angles in the theory. Unfortunately, from the TASCflow computation we have no efficiency values.

The linear methods compute higher values at the efficiency maximum than the CFD codes. One explanation migth be, that the linear methods consider no 3-D effects in the boundary layer calculation. The LBS code e.g uses a 2-D boundary layer code [23] which was developed for wings. However, the boundary layer at the fan blades, hub and duct can be considerably thicker. Especially at the duct the boundary layer can be 3 times as thick as usual which is caused by centrifugal forces. In the case of a rotating cylinder the boundary layer thickness related on the tip radius is [24]:

$$\frac{\delta}{r} = \frac{0,526}{Re^{0,2}} \tag{1}$$

Six different conditions were applied to the boundaries of the domain. The inlet boundary was modeled using the specification of total pressure corresponding to atmospheric conditions to simulate the fan drawing air from the atmosphere. The required mass flow rate were applied to the outlet boundary. The fan blades as well as the represented inner surfaces of the hub and ring were modeled as smooth turbulent walls. The radial ($r = R_{hub}$, $r = R_{tip}$) boundaries of the upstream and downstream regions have been modeled as slip walls, or frictionless walls.

Finally, the remaining boundaries of the upstream and downstream region were specified as periodic boundaries in order to simulate the effect of the adcent blade passages. Singular regions were specified as coalescence boundaries.The linearized discrete algebraic equations resulting from the finite volume approach are solved by using an Algebraic Multigrid method (AMG) based on Additive Correction Multigrid (ACM) strategy. The AGM approach uses blocking of fine grid finite volumes by imposing flux conservation over these blocks. Blocking is designed for efficient error reduction under application of an Incomplete Lower Upper (ILU) factorization (solver) relaxation scheme through a hierarchy of grids.

Fan performance

Originally the FLOWer code was developed for aviation with essential higher Mach numbers. Here we have an in-duct flow at low Mach numbers which can be less than .1.

Fig. 4 presents the measured and computed results of the static pressure. The Euler calculation results of the FLOWer code are about 25 % higher than the viscous calculated values what seems to be realistic. All the CFD computed results differ significantly at the free stream condition. For this higher flow rates the curves are diverging, because the boundary conditions are different. The real flow seems to be separated for all flow rates which is probably caused due to the sharp gradients of the hub and duct inlet geometry. Contrary to the experiment, the numerical simulation models an undisturbed onset flow. Therefore, the Navier Stokes code models a partly attached flow at higher flow coefficients, whereas the real flow is more or less separated. For higher static presssures the numerical results indicate an increased separated flow too. The same behaviour follows from the results of the turbulent computation using Bladwin-Lomax turbulence model. Generally, the transition from a partly attached flow to an increased separated flow is characterized by a slight change in the slope. Around flow coefficient of .10 which is close to the measured maximum of the efficiency the laminar computed FLOWer results agree excellent with the experiment. Towards higher static pressures the turbulent computed FLOWer data agree better with the experiment than the laminar computed values. This indicates a transition from laminar to turbulent flow around a flow coefficient of .10.

The TASCflow computation of turbulent flows leads to an overprediction of 25 % as is shown in the case of the inviscid Euler computation. This can be caused by the use of a too short inlet geometry where viscous effects are probably neglected. The boundary layer of the duct can be 3 times as thick as on the blades and insofar the duct and the hub have a strong influence on the losses of the performance.

Fig. 4 (b) compares the linear computed measured performances. The LBS code, which models the real fan geometry, overpredicts the experimental results.The slop is well predicted. The flow coefficient for the free stream condition, where the static pressure equals zero, is overpredicted by about 7 %. This can be matched by an additional pitch of about 0.8 degree only.
A similar result is obtained with the radial equlibrium method RE. Here the method is assum-

thogonal and curvilinear. Physical coordinates x, y and z locate grid nodes throughout the domain. At each node dependent variables are calculated and associated with such a cell in a wacalled collocated storage. With the use of Cartesian velocity components as dependent variables such an approach can ensure strong conservation of momentum. The logical (storage) indexing of the grid nodes through triads i,j,k lead to the so called structured characteristics of the grids used. 71 x 51 x 21 node points are used for the improved flow resolution and accuracy. The grid has a so-called Z-Topology which includes singularity points [22].

RESULTS AND DISCUSSION

Validation of the Navier Stokes Code FLOWer for Lowspeed Fans

CFD input data, convergence acceleration technique and time history

The DLR Navier Stokes computations were carried out on the NEC vector computer SX4. The initial flow data were specified as free stream values, formulated as axial and rotational Mach number. The charachteristic Reynolds number ranges from 90.000 at the hub up to 225.000 at the tip. Hub, duct and blade surface are defined as no-slip boundaries. The solution procedure uses the full multigrid technique to accelerate the numerical convergence. Here the computation starts with the coarse grid, and then interpolates the solution to the fine grid. After about 2500 cycles the solution is steady. Fig. 3 (a) represents the convergence history of the FLOWer code computation The CPU time for one complete computation is about the half of a CPU-hour.

With the TASCflow code a modified finite volume approach is applied to achieve a convergent and steady solution of the flow equations. Integral values are obtained in conservation form for fluxes of conserved quantities over control surfaces and volumes defined by the computational grids used. To advance the numerical solution process a first order backward Euler approximation of the transient term is used.

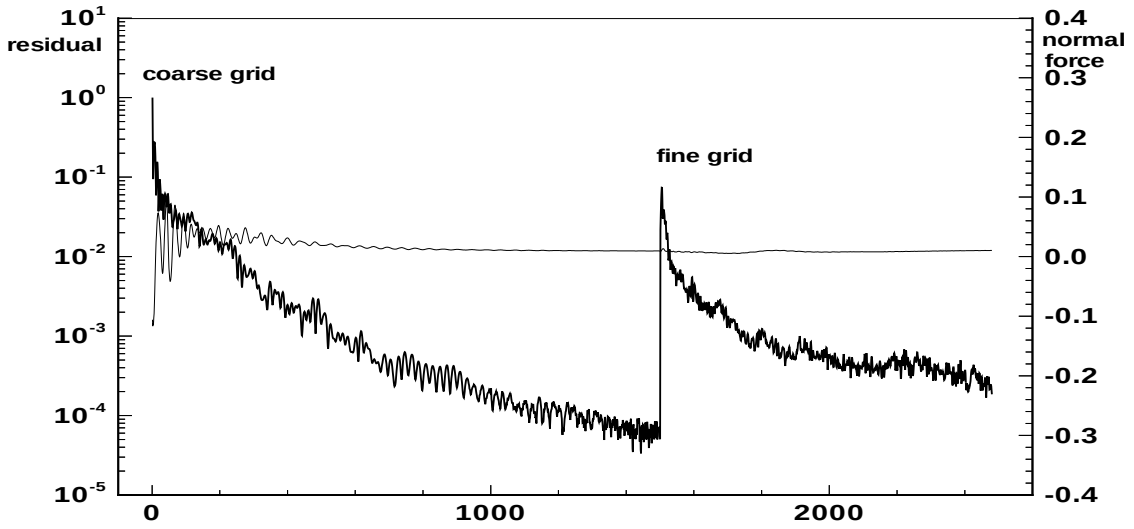

Fig. 3 Time history of the normalized residual and normal force coefficient of the DLR code FLOWer

The Radial Equilibrium Method RE

In addition to both Navier-Stokes methods and the LBS code a simple approximate method was used to determine the fan performance. This method combines radial-equilibrium calculations for the fan trailing edge plane with blade-to-blade calculations on non-axisymmetric, that means twistedstream surfaces. Twisted stream surfaces have been expected because of the considerable sweep and dihedral of the blading, introduced for acoustic reasons. Key-informations for the present method to give reasonable results are informations on the flow exit angles and the profile losses at the various radii. For fans of the usual geometry (low solidities, highstagger angles) these informations are not easily available and have to be deduced from equivalent informations on lift- and drag-coefficients, after first having been corrected for small but non-negligible interference effects. This is precisely what has been done in the present investigation.

Grid generation

The panel grid for the lifting surface code LBS models the nascelle and duct geometry as was used in the experiments. Fig. 2(a) shows the 7-bladed ducted fan with symmetrical spaced blades. The blades show a relative strong forward sweep. Altogether 2x(19x9x7) panels are used for both, the blades and the hub/duct surface.

For the CFD-computations an axisymmetric model is used and the computational domain is reduced to coaxial cylindrical surfaces, including the hub and the duct. The duct/hub length at the in- and outlet is about one chord length. For the 2-D C-Grid generation the DLR grid generator MEGACADS was used. The 3-D grid was developed by wrapping the 2-D Navier-Stokes Grid with C-topology, generated for each of the 41 radial stations separately, on a cylinder (see Fig. 2(b)). The complete 3-D DLR grid has a size of 241x65x41 grid points, where 241 grid points are distributed in blade chordwise direction, 65 grid points in blade normal direction and 41 grid points in spanwise direction.

The computational grids used for the TASCflow code are boundary-fitted, generally non-ory

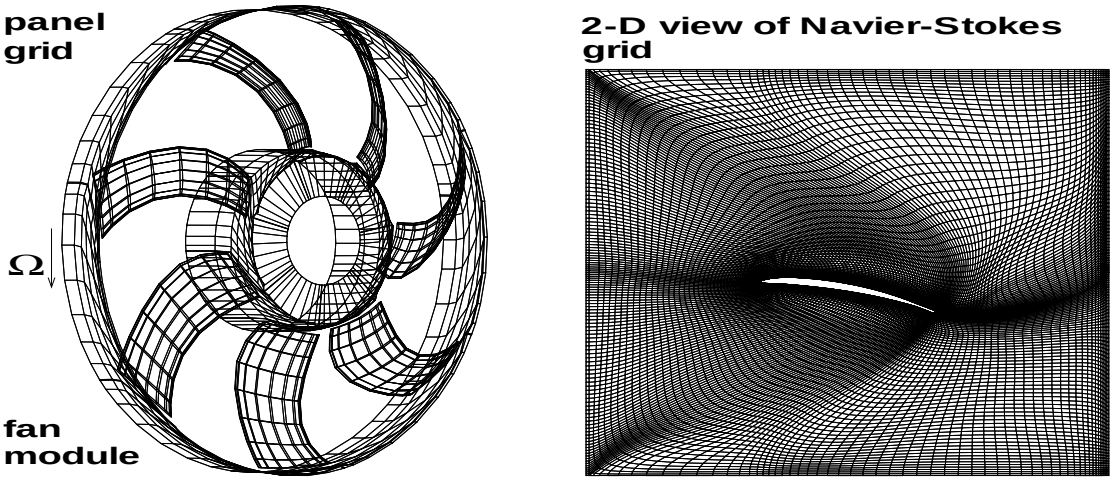

(a) (b)

Fig. 2 Used grids, (a) panel grid for LBS code, (b) CFD grid for Navier Stokes code FLOWer

as fan geometry, flow velocity, boundary layer displacement thickness, far-field distance etc. The code takes care for different noise sources caused by inflow turbulence, trailing edge and wake phenomena and blunt body effects [2].

The DLR CFD-Code FLOWer

The DLR flow simulation code FLOWer is a finite-volume solver for the solution of the three-dimensional Reynolds-averaged Navier-Stokes equation on arbitrary moving coordinate systems and flexible grids [17]. The Code is restricted to rigid body motions with three translatorial and rotational degrees of freedom. An explicit time discretization is used, and the resulting set of coupled non-linear equations is solved iteratively. This is accomplished using well proven convergence acceleration techniques for explicit schemes such as multigrid, residual averaging, and local time stepping, in order to achieve large computational efficiency in the calculation. In FLOWer the cell-vertex approach is realized.

The spatial discretization leads to an ordinary differential equation for the rate of change of the conservative flow variables in each grid point where the residual represents the approximation of the inviscid and viscous net fluxes and the source term for a particular control volume . The fluxes are approximated using a central discretization operator. In the cell-vertex formulation the update of the flow variables in the grid node is a function of the discrete flux balances of the surrounding eight cells. For the far-field boundary the freestream condition is selected. For viscous flow, two options are used for the computation: laminar and turbulent flow. Turbulence is modeled by Baldwin-Lomax turbulence model with Degani-Schiff modification for vortex flows. Therefore, in both cases of laminar and turbulent computations it is possible to treat separated flow. The multibladed fan is computed by using the periodicity condition to treat only 1 segment of $2\pi/N$ (N = number of blades).

For the application of the acoustic methods an interface is defined. This interface allows to extract pressure data from the aerodynamic solution on planes of the aerodynamic grid. The output can be used as input for the acoustic code APSIM (Acoustic Prediction System based on Integral Methods). The methods included are the linear acoustic analogy according to Farassat 1 and 1A and the Kirchhoff method. The code is the work of former code development at DLR [2,18,19]

The Siemens CFD-Code TASCflow

The air flow - driven by an axial flow fan - is modeled with a CFD software package TASCflow as an incompressible, Newtonian gas with constant properties. This simplification is justified since all calculated Mach numbers are in the range $0 < Ma < 0.2$ for the rotational speeds and dimensions considered. The used CFD tool has capabilities to solve the equations for the conservation of mass, momentum and energy in terms of the dependent variables velocity, pressure and enthalpy. Because no heat-exchange processes take place considered only the equations for mass and momentum have been solved. Turbulent flow has been assumed throughout all situations simulated. Therefore instantaneous values of scalars are obtained through Reynolds-Stress averaging of the momentum equations. Reynolds Stresses and turbulent energy fluxes are related to mean flow variables using an eddy viscosity assumption. The k-e turbulence model of Launder and Spalding provides closure to the set of equations that model the flows under consideration [20, 21].

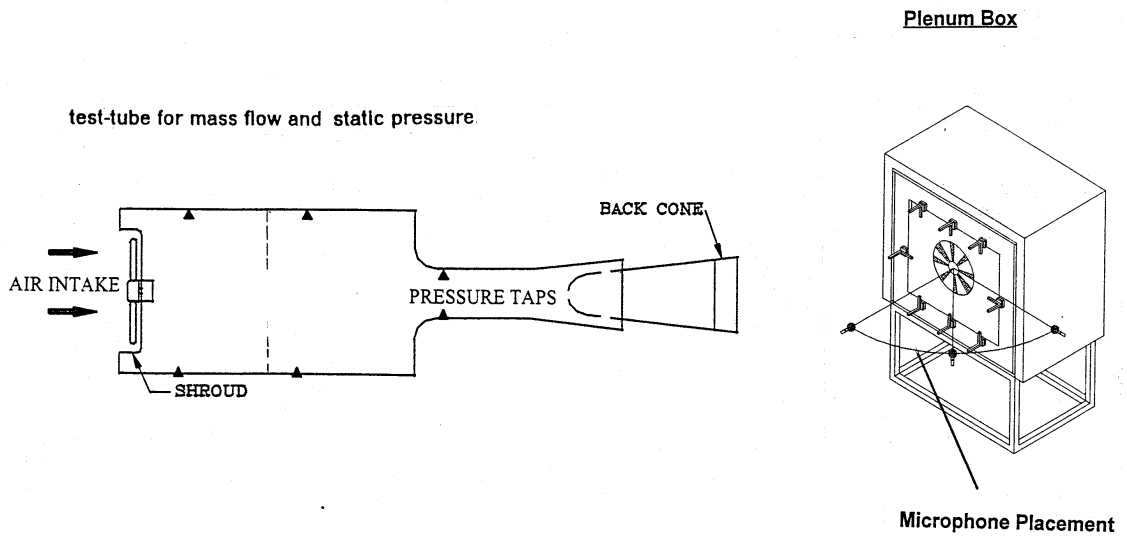

(a) (b)

Fig. 1 Siemens Electric Ltd. test facilities, (a) test tube for mass flow and static pressure (1x1 m cross section), (b) test rig of the semi anechoic chamber (6.3x5.9x3.5 m).

COMPUTATIONAL METHODS

The DLR Lifting Surface Code LBS

The governing equation is an integro-differential equation which can be obtained by integrating the FWH-equation with respect to time [2]. For computing the aerodynamic presssures the surface has to be subdivided into panels. The induced velocities are obtained by spatial differentiation. At the body surface the sum of all normal induced velocities together with the normal component of the onset flow is zero, which leads to the boundary condition and to a system of equations. The solution of the equation system gives the aerodynamic pressure distributions. To calculate the viscous flow of ducted fans, the potential field has to be modeled by monopoles, dipoles and quadrupoles, where the quadrupole disturbance velocities tangential to the airfoil contour are calculated from a boundary layer code to compute the boundary displacement thickness.

Differentiation of the potential formulation with respect to time gives the acoustic pressure integral equation which differs from Farassat formulation 1 [15] only by the boundary layer term, which can be derived from the quadrupol term. The intregrals have to be calculated at emission time. The integral equation is used to compute the periodic part of the acoustic near-field at the fan face. At the fan face nearby the rotor satisfying phase correlations can be obtained. From the gradient of the sound pressure normal to the fan face the acoustic far-field can be calculated using Rayleigh‘s formula according to the radiation from a piston in a plane wall [16].

In several cases broadband noise can dominate the overall fan noise level. Therefore, the LBS code was extended to calculate the power spectrum of stochastic noise sources based on turbulence models. The sources are located on panels. Several parameters are considered in the code

be employed to optimize the fan geometry. The fan of this study is isolated and has a rotating duct. Therefore, guide vanes and tip clearence effects [13,14] don‘t have to be considered. However, blade parameters like twist, chord, sweep or asymmetric blade staggering and blade number have to be optimized by the methods mentioned above [2,3]. Furtherly, the noise at the source can be reduced by avoiding flow separation. Here finally a CFD analysis can help to accomplish the improved design.

An essential condition to fullfil the tasks of such an optimized aeroacoustic design are excellent validated codes. Although validated codes for fan aeroacoustics are not the state of art at the time. Therefore, the goal of this study is to

1. validate the Navier Stokes Code FLOWer for lowspeed fans.

Comparisons are carried out with computational results of the code TASCflow of Siemens Electric Ltd. and their experimental data. An additional analysis of an aft swept fan should show that the FLOWer code is capable to predict all the special aerodynamic features of a forward and aft swept lowspeed fan. A further goal of this study is to

2. validate the lifting surface code LBS for local aerodynamic data as pressure, boundary layer thickness, lift and drag distributions which are required for the computation of acoustics.

The local aerodynamic data can be obtained from the Navier Stokes analysis. For the comparison experiment/theory in acoustics experimental data from Siemens Electric Ltd. is available.

DESCRIPTION OF TESTS

Experimental measurements of the aerodynamic and acoustic performance for the 390 mm axial flow fan have been conducted at Siemens Elektric Ltd in London. The fan performance was measured in a test tube of 1 x 1 m cross section where the fan sucks air from the tube which can be continously throttled down to control the airflow (see Fig. 1(a)). When the test commences, the cone is moved inward to close the nozzle outlet. The fan test program calculates equal test points from fully open to close. The cone is then moved to the calculated points and measurements are recorded.

For acoustics the testing has been conducted in a semi anechoic test chamber of 6.3 x 5.9 x 3.5 m in size with the test rig shown in Fig. 1(b). The chamber has provision to test vehicles for noise and vibration. The floor of the chamber partly consists of a concrete hard surface, providing reflection to sound fields. The background noise level is 25 dB(A). The test rig box is made of wood and surface treated with absorbent material. (The Institute of Noise Control Engineers of USA has recommended specifications for such a box).

The fan module can be tested either in a free blow or with a resistive system installed. As test conditions two operating speeds of 2800 and 3500 rpm‘s and three radial distances of .5, 1.0 and 1.5 m were selected. For each speed and radius the measuring locations were spaced over a range of 90^{o}. The test results have been recorded as Overall Sound Pressure, Narrow Band and 1/3 octave band noise level. The radial distance is measured from the origin located at the upstream face of the motor shaft. Microphones were positioned stepwise over the meshed ground of the semi-anechoic chamber.

an acoustically optimized geometry without any loss in performance. Many wind tunnel tests and numerical simulations have been conducted to improve the physical understanding of rotor aeroacoustics and to validate the aerodynamic and acoustic codes for the prediction of fan noise. From the point of industrial view a lot of additional boundary conditions have to be taken into account for fan design as a small size, no stator, low production costs, suitable for recycling, no air losses and a white noise sound with no stressing tones.

The aeroacoustic computation of a complete cooling system which consists of one or more parallel or in line working fans is very complicated. Many additional sound sources are introduced by the cooler, ducts behind or parallel to the fan, sharp wedges, changes of the cross section, gaps and slots, irregular shaped in and outlets, which are sometimes covered with a grid. Here the numerical simulation can essential be reduced, when each fan is considered isolated with an disturbed onset flow. Isolated ducted fans can be computed with the classical 2-D cascade flow method or with modern 3-D singularity or field methods. In the subsonic range the non-linear effects can be neglected and therefore the computational results of all the methods mentioned above should be approximately the same. Because of great expenses in grid generation and computer time it seems to be reasonable to use linear methods as the DLR lifting surface code or the radial equilibrium method RE for cascade flow for the numerical optimization. On the other side, only a field method as the Navier Stokes code FLOWer from DLR or TASCflow used by Siemens Electric Ltd. can compute separated flow. Therefore, for a more special analysis field methods have to be used after the design. In this way design time, expensive fan models and wind tunnel tests can be saved.

Great experience exists at DLR in the design of aeroacoustically optimal working propulsion systems using supersomputers. Panel and field methods were applied to compute propellers and rotors. The methods were developed in the early eighties and validated within the European GARTEUR activities (GARTEUR = Group of Aeronautical Research and Technology in Europe) [1]. During the last decade DLR made a technology transfer of rotor aerodynamics and acoustics from aviation to the car industry. Here the DLR lifting surface code LBS for rotors was extended to isolated ducted lowspeed fans. Additionally, another code for stochastic noise from randomly fluctuating forces was developed. Both codes were coupled with an optimization code to design aeroacoustically fans [2,3].

During the last 5 years a lot of investigations were made in the field of high speed fans respectively turbomachines, where the acoustic field is calculcated from a hybrid computational aerodynamic-aeroacoustic technique (CAA) [4, 5, 6, 7, 8, 9]. With the input of near-field aerodynamics, calculated from a Navier-Stokes CFD Code and a modal pressure analysis according to the theory of Tyler and Sofrin [10], firstly the propagating sound field around the fan is computed by using a Galerkin finite element procedure. Then secondly, at an interface relatively far away from the fan, the decaying pressure modes are input for a velocity potential formulation using a finite difference or higher order finite volume scheme. Outside the fan the essential acoustic signals are captured by a Kirchhoff integral to compute the acoustic far-field. Each acoustic mode has to be calculated separatly. Duct lining can be treated. For the treatment of acoustically absorbing liners in ducted fans also boundary element methods have been developed, which seem to be appropriate as a design tool [11,12].

Ducts of low speed radiator fans are usually too short for the implementation of lining materials. Radiator fans should also have light weight and low production costs. Therefore, in general the radiator fan noise can be only reduced at the source. For this reason a simpler analysis can

CFD-ANALYSIS OF FAN AEROACOUSTICS - COMPARATIVE STUDIES

D. Lohmann, H. Capdevila *), U. Stark **), M. Kuntz

DLR, Institute of Design Aerodynamics, Numerical Methods of Aerodynamics,
Lilienthalplatz 7, 38108 Braunschweig, Germany
*) Siemens Electric Ltd., Aerodynamics & Systems, Engine Cooling,
Automotive Syst., 1020 Adelaide Str. South, London, Ontario, N6E 1R6 Canada
**) Technical University of Braunschweig, Institute of Fluid Mechanics, Aerodynamics of Turbo Engines, Bienroderweg 3 D-38106 Braunschweig, Germany

ABSTRACT

The need of aeroacoustically highefficient fans requires more detailed investigations of three dimensional effects and separated flow analysis. Comprehensive studies and code validation for fans have shown, that further development - especially for the influence of sweep - is necessary. Therefore, two different Navier-Stokes Codes, a lifting surface code and a classical method for 3-D cascade flow were used to compute a ducted swept radiator fan. The results of the method are checked against each other and compared with experiments to firstly validate the codes in aerodynamis and secondly deliver data for acoustic calculations. Here the aerodynamic pressure and boundary displacement thickness are taken for the acoustic field computations at the fan face using the acoustic analogy method. The far-field is computed by the use of Rayleighs‘s formular.

Different flow rates were modeled for a 7-bladed fan geometry. The computational results of static pressure and efficiency are compared with experimental data. Indicated flow separation of both, a forward and an aft swept fan have been analysed. The effect of turbulence modeling and different grid size has been investigated. The linear methods used for the aeroacoustic fan design are validated for local data. In order to check the prediction capability of the DLR acoustic methods, acoustic spectra of periodic and stochastic noise parts have been calculated at different angles around the fan face and compared with measured data.

INTRODUCTION

In the past intensive research work has been carried out by the German industry and the universities to reduce lowspeed fan noise of air conditioning systems and engine cooling fans due to